



Crystallographic characterization of the palladium(I) dimers, *syn*-Pd₂Cl₂(dppmMe)₂ and Pd₂Cl₂(dppm)₂; solution conformational behavior of *syn*- and *anti*-Pd₂Cl₂(dppmMe)₂ and their (μ-Se) adducts [dppmMe = μ-1,1-bis(diphenylphosphino)ethane, and dppm = μ-bis(diphenylphosphino)methane]

Gábor Besenyei^{a,*}, László Párkányi^a, Eszter Gács-Baitz^a, Brian R. James^{b,*}

^a Chemical Research Center, Institute of Chemistry, P.O. Box 17, 1525 Budapest, Hungary

^b Department of Chemistry, The University of British Columbia, Vancouver, Canada V6T 1Z1

Received 2 June 2001; accepted 4 July 2001

This paper is dedicated to Kees Vrieze, a close friend and colleague for 35 years (at least for BRJ), for his contributions to organometallic and coordination chemistry, particularly of Pd

Abstract

An X-ray diffraction study on *syn*-Pd₂Cl₂(dppmMe)₂, *syn*-**1**, shows an unusual boat-like conformation of the eight-membered Pd₂P₄C₂ ring. This conformation, containing equatorial Me groups, facilitates access of the Pd–Pd bond to small molecules such as CO, SO₂, and elemental sulfur or selenium, and makes the *syn* isomer more reactive than *anti*-**1**. A comparison of bond angles around the Pd and P atoms in the *syn*- and *anti*-isomers reveals a more strained geometry of the former, which may also contribute to the stronger propensity of *syn*-**1** to form A-frame adducts. Solution NMR/NOE studies on *syn*- and *anti*-**1** and their (μ-Se) adducts reveal the structural rigidity of these complexes; the Me groups inhibit the interchange of axial and equatorial positions on the bridging methine C-atom, and solution structures correspond to those in the solid state. The X-ray structure of Pd₂Cl₂(dppm)₂ is, as expected, like that of the corresponding bromo complex; both are analogous to that of *anti*-**1** which adopts a chair conformation within both the fused, five-membered rings. © 2002 Elsevier Science B.V. All rights reserved.

Keywords: Palladium complexes; A-frame complexes; Selenium compounds; Bis(diphenylphosphino)methane; 1,1-Bis(diphenylphosphino)ethane

1. Introduction

The chemistry and structural characterization of complexes possessing an M₂(dppm)₂ core¹ are well developed [1]. Complexes with metal–metal bonds and mutually *trans*-dppm ligands (side-by-side complexes) generally prefer the chair-like conformation of the eight-membered M₂P₄C₂ ring if no other bridging groups are present; the same is true for face-to-face

complexes which again have mutually *trans*-μ-dppm ligands, but have no metal–metal bonding or other bridging ligands. Introduction of a third bridge, however, generates the so-called A-frame structures in which the steric demands of the dppm Ph groups disfavor the chair conformation, and typically generate boat-like conformers with the dppm methylenes bent towards the atom(s) in the apical position. However, there are a few exceptions to these generalities [2].² For example, the M₂P₄C₂ backbones in the side-by-side

* Corresponding authors. Tel.: +1-604-822 6645; fax: +1-604-822 2847.

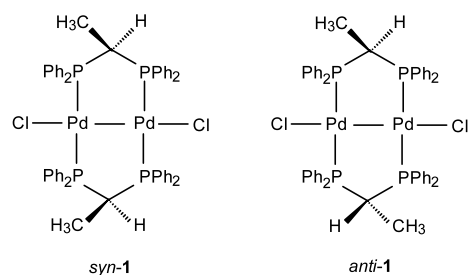
E-mail addresses: besenyei@cric.chemres.hu (G. Besenyei), brj@chem.ubc.ca (B.R. James).

¹ Throughout this paper, dppm and dppmMe refer exclusively to ligands bridging the two metal centres.

² A search in CSD (October 2000) revealed 353 structures satisfying the connectivity (C)(C)PCP(C)(C)MP(C)(C)CP(C)(C)M, where M = Rh, Ir, Ni, Pd, or Au. An additional 18 complexes were found when one or both H-atoms of the dppm methylene were replaced by substituents (M = transition metal).

complexes like $\text{Pd}_2(\text{CF}_3\text{CO}_2)_2(\text{dppm})_2$ [3], $[\text{Au}_2(\text{dppm})_2]^{2+}$ [4] and *syn*- $\text{Ir}_2\text{Cl}_2\text{I}_2(\text{CO})_2(\text{dppm})_2$ [5] adopt a boat conformation in the solid state, and the face-to-face cation $[\text{Pt}_2\text{Me}_2(\text{CO})_2(\text{dppm})_2]^{2+}$ has a boat conformation with methylene groups bending towards the Me groups located on the same side of the $\text{Pt}_2\text{P}_4\text{C}_2$ ring [6]. The complexes $[\text{Pt}_2(\text{Me})_2(\mu\text{-H})(\text{dppm})_2]\text{PF}_6$ [7] and $\text{Os}_2(\mu\text{-O})\text{Cl}_6(\text{dppm})_2$ [8] demonstrate that the presence of a third bridge does not necessarily result in a A-frame structure if the steric interactions between the apical bridge and the Ph groups are weak, and consequently these derivatives form a chair and not the expected boat conformation. The complex $\text{Pd}_2(\text{CF}_3\text{CO}_2)_2(\mu\text{-CO})(\text{dppm})_2$ appears to be the only A-frame that adopts a chair conformation [9]. Another type of irregularity is shown by $[\text{Rh}_2\text{Cl}_2(\mu\text{-pz})(\text{dppm})_2(\text{t-BuNC})_2]\text{PF}_6$ [10a] (pz = pyrazolate) and $\text{Pd}_2\text{R}_2(\mu\text{-Br})(\text{dppm})_2$, R = mesityl, [10b] in which both methylene groups are bent away from the μ -apical ligand.

We [11–14] and others [15,16] have added an extra dimension to conformational studies on dppm-type systems by replacing one of the methylene H-atoms by Me; the ligand is then 1,1-bis(diphenylphosphino)ethane, abbreviated as dppmMe to signify the methylated dppm. Our initial interest in this ligand evolved from the possibility of immobilizing a Pd₂ moiety akin to $\text{Pd}_2\text{Cl}_2(\text{dppm})_2$ (**2**) on a polystyrene support for use in separation of gases [12]. The $\text{Pd}_2\text{Cl}_2(\text{dppmMe})_2$ complex now gives rise to both *syn*- and *anti*-isomers, depending on the disposition of the Me groups with respect to the Pd–C–Pd plane.



We have established the reactivity order **2** > *syn*-**1** > *anti*-**1** for the formation of A-frame species with $\mu\text{-CO}$, $\mu\text{-SO}_2$, and $\mu\text{-X}$ (X = S or Se, formed from H_2X , or elemental S or Se), and rationalized the findings on steric arguments [13,14], based largely on structural data for *anti*-**1** [12] and *anti*- $\text{Pd}_2\text{Cl}_2(\mu\text{-Se})(\text{dppmMe})_2$ [14]. The present paper is in part not only a mini review but also reports new X-ray structural data for *syn*-**1** and **2**, which allow a more definitive discussion of the structure–reactivity relationship, as well as NMR/NOE data on *syn*- and *anti*-**1** and their $\mu\text{-Se}$ adducts, which reflect on the solution structures.

2. Experimental

Details for the syntheses of *syn*- and *anti*- $\text{Pd}_2\text{Cl}_2(\text{dppmMe})_2$ (**1**) [12,13], $\text{Pd}_2\text{Cl}_2(\text{dppm})_2$ (**2**) [12,17a], and *syn*- and *anti*- $\text{Pd}_2\text{Cl}_2(\mu\text{-Se})(\text{dppmMe})_2$ (to be abbreviated *syn*-**1**($\mu\text{-Se}$) and *anti*-**1**($\mu\text{-Se}$), respectively) [11,13,14] have been published. Orange crystals of *syn*-**1** (platelets) and **2** (prisms) were grown from CH_2Cl_2 solutions of the complexes by layering with EtOH. Some details of the crystal data, data collection and refinement details for these complexes are presented in Table 1. Intensity data were collected at 293 K on an Enraf–Nonius CAD4 diffractometer. Unit cell parameters were determined by least-squares of the setting angles of 25 reflections (*syn*-**1**: $12.99 \leq \theta \leq 13.94^\circ$; **2**: $27.10 \leq \theta \leq 29.50^\circ$). The intensities of three standard reflections were monitored regularly (every 60 min), and were corrected for decay [18]. A psi-scan absorption correction [19] was applied to the data. The structure was solved by direct methods [20] and subsequent difference syntheses. Anisotropic full-matrix least-squares refinement [21] on F^2 was carried out for all non-hydrogen atoms. H-atom positions were calculated from assumed geometries and were included in structure factor calculations but were not refined. The isotropic displacement parameters of the H-atoms approximated from the U_{eq} value of the atom to which they were bonded (the riding model was utilized). Neutral atomic scattering factors and anomalous scattering factors were taken from Ref. [22]. Selected bond lengths and angles are given in Table 2, and the molecular structures are shown in Figs. 1 and 2.

NOE spectra were recorded at ~ 300 K on a Varian Unity Inova (400 MHz) spectrometer on 2.2×10^{-2} M CDCl_3 solutions of the complexes.

3. Results and discussion

The structure of $\text{Pd}_2\text{Cl}_2(\text{dppm})_2$ (**2**) (Fig. 2) is very similar to that of the bromo analog [23], and has the same chair-like conformation of the $\text{Pd}_2\text{P}_4\text{C}_2$ ring. Complete details of the bromo complex have neither been published nor deposited in the Cambridge database, but the chloro and bromo complexes have the same space group and very similar unit cell parameters; the major difference, besides those expected for Pd–Cl and Pd–Br bond lengths, is in the Pd–Pd bond length, which is shorter (2.667(1) Å) in **2** than in the bromo complex (2.699(5) Å), and is consistent with the weaker *trans* effect of the chlorine.

The X-ray analysis on *syn*- $\text{Pd}_2\text{Cl}_2(\text{dppmMe})_2$ (Fig. 1) confirms our earlier conclusion that this isomer has an extended boat conformation for the $\text{Pd}_2\text{P}_4\text{C}_2$ ring, with the Me groups occupying equatorial positions. One interesting feature of *syn*-**1** is the significantly shorter

Pd–Pd bond (2.569(1) Å) than in the *anti*-isomer (2.664(1) Å) [12]; indeed, this is the shortest Pd–Pd bond of all diphosphine-bridged Pd₂ and Pt₂ derivatives, which vary from 2.57 to 2.77 Å (see Table 3, Series A). Generally, the shortest Pd–Pd bond (2.488(1)

Table 1
Crystal data and structure refinement parameters for *syn*-Pd₂Cl₂(dppmMe)₂(*syn*-1) and Pd₂Cl₂(dppm)₂ (2)

	<i>syn</i> -Pd ₂ Cl ₂ (dppmMe) ₂	Pd ₂ Cl ₂ (dppm) ₂
Empirical formula	C ₅₂ H ₄₈ Cl ₂ P ₄ Pd ₂ ·2CH ₂ Cl ₂	C ₅₀ H ₄₄ Cl ₂ P ₄ Pd ₂ ·H ₂ O
Formula weight	1250.34	1070.45
Radiation and wavelength (Å)	Mo Kα, 0.71073	Cu Kα, 1.54184
Crystal system	triclinic	monoclinic
Space group	P $\bar{1}$	P ₂ ₁ /c
Unit cell dimensions		
<i>a</i> (Å)	11.974(1)	13.576(4)
<i>b</i> (Å)	13.524(1)	16.419(3)
<i>c</i> (Å)	18.197(2)	21.603(2)
α (°)	99.66(1)	
β (°)	90.25(1)	106.37(1)
γ (°)	110.83(1)	
<i>V</i> (Å ³)	2708.5(4)	4620.2(17)Å ³
<i>Z</i>	2	4
<i>D</i> _{calc} (mg m ⁻³)	1.533	1.539
Absorption coefficient (mm ⁻¹)	1.114	8.937
<i>F</i> (000)	1260	2160
Crystal size (mm)	0.35 × 0.30 × 0.05	0.30 × 0.15 × 0.15
Max/min transmission	0.9871, 0.8445	0.9901, 0.6380
θ Range (°)	2.16 ≤ θ ≤ 34.98	4.33 ≤ θ ≤ 74.89
Index ranges	−19 ≤ <i>h</i> ≤ 0; −20 ≤ <i>k</i> ≤ 21; −29 ≤ <i>l</i> ≤ 29	−16 ≤ <i>h</i> ≤ 17; −20 ≤ <i>k</i> ≤ 0; −27 ≤ <i>l</i> ≤ 0
Reflections collected	23671	9702
Completeness to 2 θ	0.99	0.965
Number of standard reflections	3	3
Decay (%)	19.0	9
Reflections observed <i>I</i> > 2 σ (<i>I</i>)	13631	7062
Independent reflections	23671 [<i>R</i> _{int} = 0.0095]	9169 [<i>R</i> _{int} = 0.0278]
Refinement method	full-matrix least-squares on <i>F</i> ²	full-matrix least-squares on <i>F</i> ²
Data/restraints/parameters	23671/52/598	9169/0/527
Final <i>R</i> indices [<i>I</i> > 2 σ (<i>I</i>)]	<i>R</i> ₁ = 0.0477, <i>wR</i> ₂ = 0.1180	<i>R</i> ₁ = 0.0639, <i>wR</i> ₂ = 0.1662
<i>R</i> indices (all data)	<i>R</i> ₁ = 0.1035, <i>wR</i> ₂ = 0.1306	<i>R</i> ₁ = 0.0813, <i>wR</i> ₂ = 0.1768
Max. and mean shift/esd	0.002, 0.000	0.001, 0.000
Goodness-of-fit on <i>F</i> ²	0.993	0.973
Largest difference peak and hole (e Å ⁻³)	2.033 and −1.542	3.307 and −1.825

Table 2
Selected bond lengths (Å) and bond angles (°) of *syn*-1, *anti*-1, and 2

	<i>syn</i> -1	<i>anti</i> -1 ^a	2
<i>Bond lengths</i>			
Pd(1)–Pd(2)	2.569(1)	2.664(1)	2.661(1)
Pd(1)–Cl(1)	2.399(1)	2.420	2.410(2)
Pd(2)–Cl(2)	2.374(1)	2.401	2.423(2)
Pd(1)–P(1)	2.291(1)	2.297	2.295(1)
Pd(1)–P(3)	2.303(1)	2.297	2.278(1)
Pd(2)–P(2)	2.320(1)	2.294	2.300(1)
Pd(2)–P(4)	2.290(1)	2.294	2.314(1)
P(1)–C(2)	1.856(2)	1.839	1.827(6)
P(2)–C(2)	1.875(2)	1.849	1.819(5)
P(3)–C(1)	1.871(3)	1.861	1.824(5)
P(4)–C(1)	1.850(2)	1.862	1.836(5)
<i>Bond angles</i>			
P(3)–C(1)–P(4)	104.1(1)	105.9	105.8(2)
P(1)–C(2)–P(2)	102.1(1)	106.5	108.7(3)
Cl(1)–Pd(1)–Pd(2)	169.02(3)	177.5	173.79(4)
Cl(2)–Pd(2)–Pd(1)	171.00(2)	177.0	178.78(4)
P(1)–Pd(1)–P(3)	171.5(1)	175.5	171.9(1)
P(2)–Pd(2)–P(4)	170.60(2)	173.4	175.5(1)

^a Data from Ref. [12].

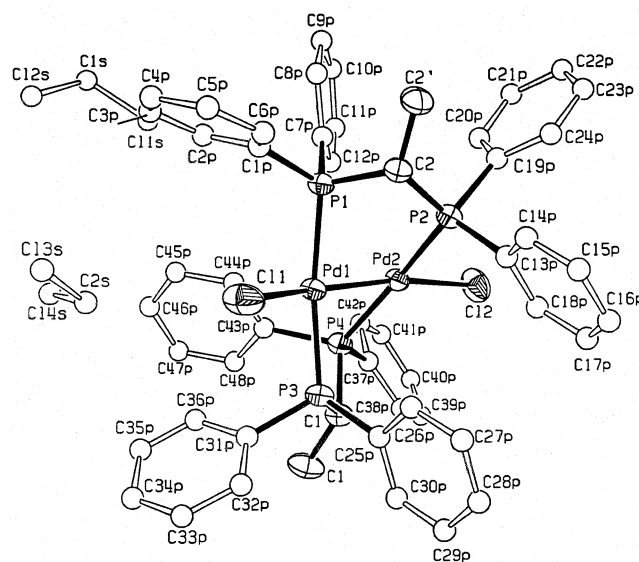


Fig. 1. Molecular diagram of *syn*-Pd₂Cl₂(dppmMe)₂ (*syn*-1) showing the numbering scheme used. Atomic displacement parameters represent 50% probabilities. H-atoms and one solvent molecule are omitted for clarity.

Å) is found in the non-bridged complex [Pd₂(MeCN)₄(PPh₃)₂]²⁺ (Table 3, Series B), while this bond is stretched to 3.185(1) Å in [Pd₂(μ-C₄H₆)₂]²⁺, which has bridging 1,3-butadiene molecules [26].

The other interesting feature of *syn*-1 is the relatively large dihedral angle (Φ) between the two coordination, least-squares planes formed by the two metal centers ($\Phi = 49.1^\circ$, see Table 3). The degree of twisting is larger than that found in *anti*-1 (37.4°) [12], and in all the other Series A complexes, except for Pd₂Br₂(dmpm)₂

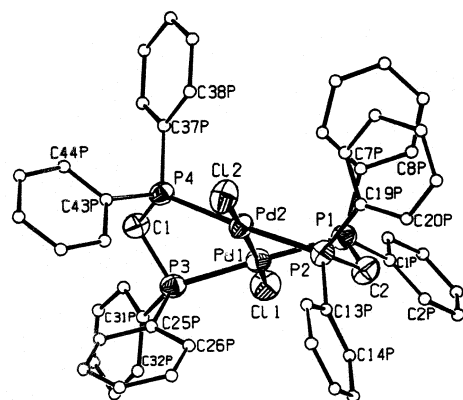


Fig. 2. Molecular diagram of $\text{Pd}_2\text{Cl}_2(\text{dppm})_2$ (**2**) showing the numbering scheme used. Atomic displacement parameters represent 50% probabilities. H-atoms and solvent molecules are omitted for clarity.

Table 3

A compilation of data for some dimeric Pd(I) and Pt(I) complexes^a

Compound	M–M (Å)	Φ (°)	Reference
<i>Series A, bis(diphosphine)-bridged complexes</i>			
$\text{Pd}_2\text{Br}_2(\text{dppm})_2$	2.699(5)	39	[23]
$\text{Pd}_2\text{Cl}_2(\text{dppm})_2$	2.661(1)	38.7	t.w.
$\text{Pd}_2\text{Cl}(\text{SnCl})_3(\text{dppm})_2$	2.644(2)	41.3	[24a]
$\text{Pd}_2(\text{C}_6\text{Cl}_5)_2(\text{dppm})_2$	2.670(2)	45.0	[24b]
$\text{Pd}_2(\text{CF}_3\text{CO}_2)_2(\text{dppm})_2$	2.594(2)	44.5	[3]
$[\text{Pd}_2(\text{HpyS})_2(\text{dppm})_2]^{2+}$	2.665(1)	40.0	[24c]
<i>anti</i> - $\text{Pd}_2\text{Cl}_2(\text{dppmMe})_2$	2.664(1)	37.4	[12]
<i>(anti-1)</i>			
<i>syn</i> - $\text{Pd}_2\text{Cl}_2(\text{dppmMe})_2$ (<i>syn-1</i>)	2.569(1)	49.1	t.w.
$\text{Pd}_2\text{Br}_2(\text{dmpm})_2$	2.603(1)	50.5	[24d]
$\text{Pd}_2\text{Cl}_2(\text{dcpm})_2$	2.646(1)	38.5	[24e]
$\text{Pt}_2\text{Cl}_2(\text{dppm})_2$	2.651(1)	38.6	[24f]
$[\text{Pt}_2\text{Cl}(\text{CO})(\text{dppm})_2]^+$	2.620(1)	40.1	[24g]
$[\text{Pt}_2\text{Cl}(\text{Ph}_3\text{P})(\text{dppm})_2]^+$	2.665(2)	42	[24h]
$[\text{Pt}_2(\text{CO})_2(\text{dppm})_2]^{2+}$	2.642(1)	40.0	[24i]
$[\text{Pt}_2\text{H}(\eta^1\text{-dppm})(\text{dppm})_2]^+$	2.769(1)	33.5	[24j]
$[\text{Pt}_2(\text{dppm})_2(\text{quin})_2]^{2+}$	2.615(1)	37.1	[24k]
$[\text{Pt}_2\text{Cl}(\text{dppm})_2(\text{tmpy})]^+$	2.627(2)	39.6	[24k]
$[\text{Pt}_2(\text{dppm})_2(\text{mim})_2]^{2+}$	2.580(1)	47.2	[24k]
<i>Series B, non-bridged complexes</i>			
$[\text{Pd}_2(\text{CH}_3\text{NC})_6]^{2+}$	2.531(1)	86.2	[25a]
$\text{Pd}_2\text{I}_2(\text{CH}_3\text{NC})_4$	2.533(1)	85.3	[25b]
$[\text{Pd}_2(\text{bipy})_2(\text{ArNC})_2]^{2+}$	2.518(3)	81	[25c]
$[\text{Pd}_2(\text{phenMe}_2)_2(\text{ArNC})_2]^{2+}$	2.599(2)	69	[25c]
$[\text{Pd}_2(\text{dppp})_2(\text{ArNC})_2]^{2+}$	2.617(2)	86	[25d]
$[\text{Pd}_2(\text{dppen})_2(\text{ArNC})_2]^{2+}$	2.602(1)	78.0	[25d]
$[\text{Pd}_2(\text{PMe}_3)_6]^{2+}$	2.598(1)	89.0	[25e]
$\text{Pd}_2\text{Cl}_2(t\text{-BuNC})_4$	2.532(2)	82.7	[25f]
$[\text{Pd}_2(\text{MeCN})_4(\text{PPh}_3)_2]^{2+}$	2.488(1)	76.3	[26]
$[\text{Pt}_2(\text{CO})_2\text{Cl}_4]^{2-}$	2.584(2)	60	[25g]

^a t.w. = this work; HpyS = 4-mercaptopyridine, bound as a thione; dmpm = bis(dimethyl-phosphino)methane; dcpm = bis(dicyclohexyl-phosphino)methane; quin = quinoline; tmpy = 2,4,6-trimethylpyridine; mim = 1-methyl-imidazole; bipy = 2,2'-bipyridine; Ar = aryl; phenMe₂ = 2,9-dimethyl-1,10-phenanthroline; dppen = *cis*-1,2-bis(diphenylphosphino)ethane.

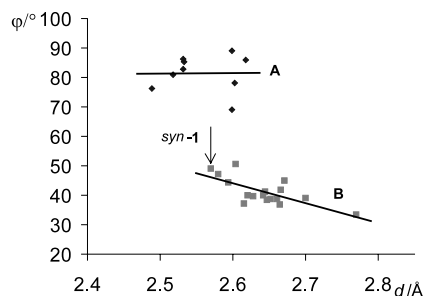


Fig. 3. Dependence of metal–metal distances on the dihedral angles of metal ion coordination planes (Φ) for bis(diphosphine)-bridged (Series A) and unsupported (Series B) Pd_2 and Pt_2 complexes.

($\Phi = 50.5^\circ$), where more severe twisting about the Pd–Pd bond was attributed to the sterically less demanding dmpm ligand (vs. dppm) [24c]. Clearly, the data presented here for *syn-1* show that the incorporation of a Me group at the methylene of dppm can also lead to increased twisting about the Pd–Pd axis. The conformation of the eight-membered $\text{Pd}_2\text{P}_4\text{C}_2$ ring most likely determines the twisting of the two PdP_2Cl coordination planes about the metal–metal bond. A model of *syn-1* in a boat conformation, with equatorial Me groups and the two P–Pd–P axes oriented parallel to each other, shows four axial Ph groups on one side of the $\text{Pd}_2\text{P}_4\text{C}_2$ ring. The resulting unfavorable steric interactions are minimized via a twisting about the Pd–Pd axis; this also minimizes the repulsive overlap of the out-of-plane, filled metal $d\pi$ orbitals [24d,25g]. These two factors are probably synergistic, and result in a structure with an unusually large dihedral angle and a short (strong) Pd–Pd bond.

The relationship between dihedral angles and metal–metal bond lengths in Pd_2 complexes has been discussed earlier [24c,27], nevertheless, we show here more extensive data for both Pd_2 and Pt_2 complexes (Table 3, Fig. 3) that lead to more definitive conclusions. Two major factors governing Φ are: (i) the repulsive interactions of the metal $d\pi$ orbitals, which are minimal at 45° ; and (ii) the steric repulsions of ligands *cis* to the metal–metal bond, which are minimized at 90° [24c,24d,25g,27]. In agreement with this, the dihedral angles fall between 45 and 90° in ‘unsupported’, dimeric square-planar complexes (Table 3, Series B). With the exception of $[\text{Pt}_2(\text{CO})_2\text{Cl}_4]^{2-}$, where $\Phi = 60^\circ$ [25g], the dihedral angles are larger, in the 69 – 89° range; ligand–ligand repulsions clearly decide the molecular geometry, and there is no obvious relationship between Φ and the metal–metal bond length for the very diverse set of non-bridging ligand systems (Table 3, Fig. 3, line B).

On the contrary, the metal–metal bond lengths in complexes with bridging diphosphines appear to decrease with an increase in the dihedral angle (Table 3, Fig. 3, line A). That the values are in the 33 – 50.5° range suggests that the orbital repulsive interactions are dominant, although rotation around the metal–metal

bond is restricted by the bridging nature of the P–P ligand. For a fixed ring size, steric factors depending on the nature of the substituent(s) at the P-atoms, the size of the ligand *trans* to the M–M bond, and sometimes the intramolecular H-bonded interactions [27], must also play a role and could, for example, contribute to the scatter around the least-squares line A.

Besides the Pd–Pd distance, other bond lengths of *syn-1* are close to those reported for *anti-1* (Table 2). The bond angles, however, reveal the more strained geometry of *syn-1*. For example, the XPdY bond angles in *syn-1* deviate more from 90°; the differences in the largest and smallest angles around Pd(1) and Pd(2) are 12.3 and 11.1°, respectively, while the respective numbers are 2.1° and 6.7° in *anti-1*. Severe distortions from the tetrahedral geometries around P(1) and P(4) with 125.3 and 121.9° angles are seen in *syn-1*, accompanied by Pd–Pd–Cl and P–Pd–P angles of 169.5 and 171.0°, respectively, with the deviation from linearity for the *anti* isomer (177.2 and 174.5°) being much smaller.

It is noteworthy that while three of the four ‘diagonal’ Pd⋯P distances in the two Pd₂P₂C rings in *syn-1* are somewhat shorter (3.245–3.377 Å) than the sum of the van der Waals radii (3.45 Å), there are no such contacts in *anti-1* [12]. This feature resembles the interactions observed sometimes in non-bridged dimeric complexes where equatorial phosphine and isonitrile ligands are bent towards their non-bonded metal centers [25a,e]. The contacts may just result from the larger dihedral angle discussed above, as other close contacts are also apparent; e.g. in *syn-1*, [P(1)⋯P(2) 2.902 Å and P(3)⋯P(4) 2.933 Å] compared with the corresponding values of 2.955 and 2.970 Å in *anti-1*, and 2.962 and 2.919 Å in **2**.

Before solution reactivity is considered, it is important to establish the solution structures in relation to the solid-state structures discussed above. Complexes of type **2** are known to be fluxional in solution with the methylene H-atoms being rendered equivalent by a rapid interchange of the axial and equatorial positions via a ring flipping motion; the same motion also makes the Ph groups equivalent, and only one set of *o*-, *m*-, and *p*-protons is seen in ¹H NMR [17]. In order to shed light on the conformational features of Pd₂Cl₂-(dppmMe)₂ complexes in solution, ¹H NMR/NOE spectra were recorded to map the intramolecular steric interactions. The ¹H and ³¹P{¹H} NMR spectra of *syn*- and *anti-1*, and their derived μ-Se adducts (Table 4), have been reported earlier [11–13]. The assignments are straightforward: in *syn*- and *anti-1*, and *syn-1*(μ-Se), the two CH (and Me) protons are equivalent, as are the P-atoms, and virtual coupling to the remote P-atoms gives the expected splitting patterns. For *anti-1*(μ-Se), the two CH (and Me) protons become inequivalent, and coupling occurs only with the adjacent P-atoms. The ¹³C NMR spectra are reported here for the first

time (Table 4). Two sets of four Ph groups are distinguished in *syn*- and *anti-1*, and in *syn-1*(μ-Se), while four pairs of equivalent Ph rings are seen for *anti-1*(μ-Se). The enhancements of resonance induced by intramolecular dipole–dipole relaxation between interacting nuclei are given in Table 5.

For *anti-1*, irradiation of the Me hydrogens results in the enhancement of both sets of the *o*-protons, showing that the Me groups are roughly equidistant from both sets of Ph rings, i.e. they maintain their equatorial position in solution. The axial orientation of the CH protons allows steric interactions only with the *o*-hydrogens of the equatorial Ph rings, their distances from the other set of *o*-protons being much larger. These observations confirm that the conformations of *anti-1* in solution and in the solid state are the same, viz. an extended chair arrangement with equatorial Me groups. Unlike the dppm-bridged complexes [17], interchange of the axial and equatorial positions at the bridging C-atoms is hampered by the Me substituents.

The NOE difference spectra of *syn-1* reveal corresponding, intramolecular steric effects, with the conclusion that the solution conformation has equatorial Me groups, but now with an extended boat arrangement. Fig. 4, showing a superimposition of the central core of *syn*- and *anti-1* looking down the Pd–Pd axis, clearly illustrates the positioning of the equatorial Me groups in both isomers.

The NMR spectra of *syn-1*(μ-Se) (see above) reveal the C_{2v} symmetry of the solution geometry, but do not give information on whether the equivalent Me groups are equatorial or axial. The NOE spectra, however, reveal dipole–dipole interactions of the CH-hydrogens only with one set of the *o*-hydrogens, while both sets of *o*-protons give NOE effects when the Me resonance was saturated; the Me groups thus maintain their equatorial orientation in the (μ-Se) derivative within an extended boat conformation. This conserved orientation, evident in solution reactivity, is readily pictured as it involves no steric interaction of the approaching reagent with axially oriented Me groups, and is the major factor making *syn-1* more reactive than *anti-1* (see below).

The reaction of *anti-1* to form *anti-1*(μ-Se) results in a change from a chair into boat conformation, and one of the Me groups flips from an equatorial to axial position [14]. Accordingly, the equatorial Me in *anti-1*(μ-Se) interacts with two sets of *o*-hydrogens, while the other axial Me detects the proximity of only one set of *o*-protons (Table 5); consistent with this, the CH-hydrogen adjacent to the axial Me shows dipole–dipole relaxation with two sets of *o*-hydrogens (Table 5). Of the complexes studied here, this is the only case where a CH-hydrogen interacts with two sets of *o*-hydrogen atoms.

Table 4
NMR spectroscopic data for *syn*- and *anti*-**1** and their μ -Se adducts

Compound	Carbon atoms			Hydrogen atoms		
	δ_C^a	J_{CP} (Hz)	Position	δ_H^a	J_{HH}/J_{HP} (Hz)	Position
<i>syn</i> - 1	15.16 (qn)	1.6	methyl (e)	1.09 (d qn)	7.0/6.6	methyl (e)
	41.64 (qn)	9.8	methine	4.84 (q qn)	7.0/5.5	methine (a)
	aromatic carbons			set 1		
	135.90		n.a.	7.54		<i>ortho</i>
	132.85		n.a.	7.33		<i>para</i>
	130.92		quaternary	7.16		<i>meta</i>
	130.59		n.a.	set 2		
	129.68		quaternary	7.63		<i>ortho</i>
	129.63		n.a.	7.31		<i>para</i>
	128.18		n.a.	7.23		<i>meta</i>
127.69		n.a.				
<i>anti</i> - 1	15.02 (m)		methyl (e)	1.05 (d qn)	6.8/6.1	methyl (e)
	42.22 (qn)	9.0	methine	4.94 (q qn)	6.8/6.2	methine (a)
	Aromatic carbons			set 1		
	137.01		n.a.	7.76		<i>ortho</i>
	132.81		n.a.	7.46		<i>para</i>
	132.00		quaternary	7.45		<i>meta</i>
	130.54		n.a.	set 2		
	129.70		n.a.	7.22		<i>para</i>
	129.47		quaternary	7.13		<i>ortho</i>
	128.45		n.a.	6.80		<i>meta</i>
127.36		n.a.				
<i>syn</i> - 1 (μ -Se)	14.87 (b, m)		methyl (e)	0.98 (d qn)	7.2/6.1	methyl (e)
	30.65 (qn)	14.7	methine	5.61 (q qn)	7.2/7.3	methine (a)
	Aromatic carbons			set 1		
	132.48 (4C)		quaternary			
	132.10 (8C)		<i>ortho</i>	7.71		<i>ortho</i>
	129.69 (4C, bs)		<i>para</i>	7.34		<i>para</i>
	128.43 (8C)		<i>meta</i>	7.33		<i>meta</i>
	set 2					
	136.74 (8C)		<i>ortho</i>	7.54		<i>ortho</i>
	130.64 (4C)		<i>para</i>	7.32		<i>para</i>
127.39 (8C)		<i>meta</i>	7.21		<i>meta</i>	
127.3 (4C)		quaternary				
<i>anti</i> - 1 (μ -Se)	14.74 (t)	3.8	methyl (e)	0.98 (d t)	7.2/10.1	methyl (e)
	30.37 (t)	26.7	methine	5.88 (t q)	7.2/13.8	methine (a)
	Aromatic carbons			set 1		
	132.17 (4C)		<i>ortho</i>	7.89		<i>ortho</i>
	131.9 (2C)		quaternary			
	129.83 (2C, bs)		<i>para</i>	7.47		<i>para</i>
	128.67 (4C)		<i>meta</i>	7.48		<i>meta</i>
	set 2					
	137.01 (4C)		<i>ortho</i>	7.38		<i>ortho</i>
	130.62 (2C, bs)		<i>para</i>	7.23		<i>para</i>
127.32 (4C)		<i>meta</i>	7.02		<i>meta</i>	
126.6 (2C)		quaternary				
21.99 (t)	3.0	methyl (a)	1.38 (d t)	7.1/13.0	methyl (a)	
37.38 (t)	22.2	methine	4.08 (m)		methine (e)	
Aromatic carbons			set 3			
137.32 (4C)		<i>ortho</i>	7.92		<i>ortho</i>	
132.3 (2C)		quaternary				
130.62 (2C, bs)		<i>para</i>	7.37		<i>para</i>	
127.90 (4C)		<i>meta</i>	7.32		<i>meta</i>	
set 4						
134.34 (4C)		<i>ortho</i>	7.66		<i>ortho</i>	
133.2 (2C)		quaternary				
129.68 (2C, bs)		<i>para</i>	7.26		<i>para</i>	
127.52 (4C)		<i>meta</i>	7.18		<i>meta</i>	

^a In ppm, relative to TMS; n.a. = not assigned; bs = broad singlet; d = doublet; q = quartet; qn = quintet; t = triplet; a = axial; e = equatorial.

Table 5
Enhancements of selected resonances in NOE difference spectra ^a

Irradiated resonances	Resonances observed					
	CH ₃		CH		o-Protons	
	δ	η	δ	η	δ	η
<i>anti-1</i>						
CH (δ 4.94)	1.05	2.1			7.76	9.9
CH ₃ (δ 1.05)			4.94	7.2	7.13	3.8
					7.76	2.4
<i>syn-1</i>						
CH (δ 4.84)	1.09	2.2			7.63	9.7
CH ₃ (δ 1.09)			4.84	7.7	7.54	4.0
					7.63	3.0
<i>syn-1</i> (μ-Se)						
CH (δ 5.62)	0.98	1.7			7.71	9.0
CH ₃ (δ 0.98)			5.62	7.9	7.55	5.2
					7.71	3.5
<i>anti-1</i> (μ-Se)						
CH (δ 5.88)	0.98	2.3			7.89	12
CH ₃ (δ 0.98)			5.88	7.0	7.38	5.1
					7.89	2.9
CH (δ 4.08)	1.38	^b			7.66	6
					7.92	3.5
CH ₃ (δ 1.38)			4.08	6.7	7.92	4.1

^a $\eta = 100 (I - I_0)/I_0$, where I is the integrated intensity for one proton.

^b Not determined.

It is noteworthy that the NOE experiments reveal an erroneous assignment regarding the Me groups and CH-hydrogens in *anti-1*(μ-Se) [14], where the δ_{Me} 1.38 and δ_{H} 5.88 resonances were assigned to geminal positions on the methine C-atom of dppmMe; the NOE data show that the δ_{Me} 0.98 is 'associated with' the δ_{H} 5.88 resonance.

The spontaneous but slow isomerization of *syn-1* to *anti-1* ($t_{1/2} \sim 15$ days in CHCl₃ at $\sim 20^\circ$) thus involves the conversion of an extended boat conformation to a chair form, with Me groups in both isomers occupying equatorial positions. The strains reflected in steric congestion in *syn-1* versus *anti-1* must contribute to this conversion, as well as to a higher reactivity of the former (see Section 1). The other key factor is the configuration adopted by the respective A-frame adducts: e.g. in *anti-1*, the Me groups occupy the less sterically crowded pseudoequatorial positions of the fused five-membered, chair conformation chelate rings [12], while in the A-frame product *anti-1*(μ-Se) both the twisted rings adopt boat conformations with the methylene C-atoms being bent towards the Se bridge and one of the Me groups is twisted into a less sterically favored axial position (inside the boat) [12].

The structure of **2** is remarkably similar to that of *anti-1* (except for the presence of the pseudoequatorial Me group) and the much higher reactivity of **2** [12] must again result from the unfavorable sterics in the

A-frame adducts formed from *anti-1* (see above). The reactivity trend: **2** > *syn-1* > *anti-1* (e.g. for the reaction with CO in CH₂Cl₂, the normalized equilibrium constants are in the following order 1: $\sim 10^{-3}$: $\sim 10^{-5}$ [13,14]) is obviously governed by the effects of the Me groups.

Essentially, formation of a boat conformer within an A-frame adduct takes place when a reagent approaches the Pd–Pd bond of any of the Pd₂Cl₂(dppm/dppmMe)₂ complexes. Irrespective of the side attacked in *anti-1*, the entering reagent will experience steric hindrance by an axial Me. In **2**, formation of the boat conformer generates only axial H-atoms. In *syn-1*, the boat conformation with equatorial Me groups is not changed during a reaction at the Pd–Pd bond, and interactions with the Me-groups are irrelevant; the steric effects of the axial Ph-groups on the other side of the Pd₂P₄C₂ plane probably make *syn-1* less reactive than **2**.

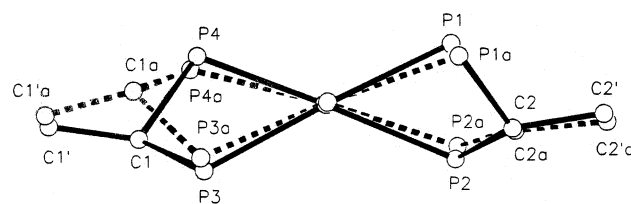


Fig. 4. A superimposition of the central core of *syn-1* (solid line) and *anti-1* (dashed line) looking down the Pd–Pd axis.

4. Summary

The structural data for $\text{Pd}_2\text{Cl}_2(\text{dppm})_2$ (**2**) and *syn*- $\text{Pd}_2\text{Cl}_2(\text{dppmMe})_2$ (*syn*-**1**) support the earlier conclusions regarding their geometries. The boat conformation of the $\text{Pd}_2\text{P}_4\text{C}_2$ ring and the equatorial orientation of the Me groups in *syn*-**1** (both in solid state and solution) have been confirmed. NOE spectra show that the Me groups retain their equatorial positions in the A-frame adduct *syn*- $\text{Pd}_2\text{Cl}_2(\mu\text{-Se})(\text{dppmMe})_2$. The higher reactivity of *syn*-**1** can be ascribed to the presence of a relatively open space about the Pd–Pd bond on one side of the $\text{Pd}_2\text{P}_4\text{C}_2$ ring, as well as possible contributions from its distorted geometry manifested by the strained bond angles at the Pd- and P-atoms. Because of steric congestion exercised by four Ph-rings on the ‘methyl side’ of the $\text{Pd}_2\text{P}_4\text{C}_2$ ring, large dihedral angles of the two metal-centered planes can be expected for *syn*- $[\text{Pd}_2\text{Cl}_2(\mu\text{-X})(\text{dppmMe})_2]$ A-frame derivatives.

5. Supplementary material

Crystallographic data for structural analysis have been deposited with the Cambridge Crystallographic Data Centre, CCDC No. 172852 for complex *syn*-**1**, $\text{Pd}_2\text{Cl}_2(\text{dppmMe})_2$ and 172851 for structure **2**, $\text{Pd}_2\text{Cl}_2(\text{dppm})_2$. Copies of this information may be obtained free of charge from The Director, CCDC, 12 Union Road, Cambridge, CB2 1EZ, UK (fax: +44-1223-336033; e-mail: deposit@ccdc.cam.ac.uk or www: <http://www.ccdc.cam.ac.uk>).

Acknowledgements

We thank the Hungarian Research Fund (OTKA Grant T 25870) and the Natural Sciences and Engineering Council of Canada for financial support, and Mr. Craig Pamplin for valuable discussions.

References

- [1] (a) R.J. Puddephatt, Chem. Soc. Rev. 12 (1983) 99; (b) B. Chaudret, B. Delavaux, R. Poilblanc, Coord. Chem. Rev. 86 (1988) 191.
- [2] F.H. Allen, O. Kennard, Chem. Des. Autom. News 8 (1993) 31.
- [3] T.E. Krafft, C.I. Hejna, J.S. Smith, Inorg. Chem. 29 (1990) 2682.
- [4] A. Bauer, H. Schmidbaur, J. Chem. Soc., Dalton Trans. (1997) 1115.
- [5] A. Crispini, M. Ghedini, F. Neve, Inorg. Chim. Acta 209 (1993) 235.
- [6] A.T. Hutton, B. Shabanzadeh, B.L. Shaw, J. Chem. Soc., Chem. Commun. (1983) 1053.
- [7] M.P. Brown, S.J. Cooper, A.A. Frew, L. Manojlović-Muir, K.W. Muir, R.J. Puddephatt, M.A. Thomson, J. Chem. Soc., Dalton Trans. (1982) 299.
- [8] A.R. Chakravarty, F.A. Cotton, W. Schwotzer, Inorg. Chem. 23 (1984) 99.
- [9] D.J. Wink, B.T. Creagan, S. Lee, Inorg. Chim. Acta 180 (1991) 183.
- [10] (a) L.J. Tortorelli, C. Woods, A.T. McPhail, Inorg. Chem. 29 (1990) 2726; (b) R.A. Stockland Jr., G.K. Anderson, N.P. Rath, Organometallics 16 (1997) 5096.
- [11] G. Besenyei, C.-L. Lee, B.R. James, Chem. Commun. (1986) 1750.
- [12] C.-L. Lee, Y.-P. Yang, S.J. Rettig, B.R. James, D.A. Nelson, M.A. Lilga, Organometallics 5 (1986) 2220.
- [13] G. Besenyei, C.-L. Lee, Y. Xie, B.R. James, Inorg. Chem. 30 (1991) 2446.
- [14] G. Besenyei, L. Párkányi, L.I. Simándi, B.R. James, Inorg. Chem. 34 (1995) 6118.
- [15] (a) A.F.M. van der Ploeg, G. van Koten, Inorg. Chim. Acta 51 (1981) 225; (b) P.A.W. Dean, R.S. Srivastava, Can. J. Chem. 63 (1985) 2829.
- [16] (a) J. Shain, J.P. Fackler Jr., Inorg. Chim. Acta 131 (1987) 157; (b) C.-M. Che, H.-K. Yip, V.W.-W. Yam, P.-Y. Cheung, T.-F. Lai, S.-J. Shieh, S.-M. Peng, J. Chem. Soc., Dalton Trans. (1992) 427.
- [17] (a) L.S. Benner, A.L. Balch, J. Am. Chem. Soc. 100 (1978) 6099; (b) A. Balch, L.S. Benner, M.M. Omstead, Inorg. Chem. 18 (1979) 2996.
- [18] K. Harms, XCAD4 Data Reduction Program for CAD4 Diffractometers, Philipps-Universität, Marburg, Germany, 1996.
- [19] (a) A.C. North, D.C. Phillips, F. Mathews, Acta Crystallogr. A 24 (1968) 350; (b) J. Reibenspies, DATCOR program for empirical absorption correction, Texas A & M University, College Station, TX, USA, 1989.
- [20] G.M. Sheldrick, SHELXS-97 Program for Crystal Structure Solution, University of Göttingen, Göttingen, Germany, 1997.
- [21] G.M. Sheldrick, SHELXL-97 Program for Crystal Structure Refinement, University of Göttingen, Göttingen, Germany, 1997.
- [22] A.J.C. Wilson (Ed.), International Tables for X-ray Crystallography, vol. C, Kluwer Academic, Dordrecht, 1992 (Tables 6.1.1.4, 4.2.6.8, and 4.2.4.2).
- [23] (a) R.G. Holloway, B.R. Penfold, R. Colton, M.J. McCormick, J. Chem. Soc., Chem. Commun. (1976) 485; (b) R. Colton, M.J. McCormick, C.D. Pannon, Aust. J. Chem. 31 (1978) 1425.
- [24] (a) M.M. Olmstead, L.S. Benner, H. Hope, A.L. Balch, Inorg. Chim. Acta 32 (1979) 193; (b) P. Espinet, J. Fornies, C. Fortuña, G. Hidalgo, F. Martinez, M. Tomas, J. Organomet. Chem. 317 (1986) 105; (c) M. Maekawa, M. Munakata, T. Kuroda-Sowa, Y. Suenaga, Inorg. Chim. Acta 281 (1998) 116; (d) M.L. Kullberg, F.K. Lemke, D.R. Powell, C.P. Kubiak, Inorg. Chem. 24 (1985) 3589; (e) M. Hashioka, K. Sakai, T. Tsobomura, Acta Crystallogr. C 54 (1998) 1244; (f) Lj. Manojlović-Muir, K.W. Muir, T. Solomun, Acta Crystallogr. B 35 (1979) 1237; (g) Lj. Manojlović-Muir, K.W. Muir, T. Solomun, J. Organomet. Chem. 179 (1979) 479; (h) R.J. Blau, J.H. Espenson, S. Kim, R.A. Jacobson, Inorg. Chem. 25 (1986) 757; (i) J.R. Fisher, A.J. Mills, S. Sumner, M.P. Brown, M.A. Thomson, R.J. Puddephatt, A.A. Frew, Lj. Manojlović-Muir, K.W. Muir, Organometallics 1 (1982) 1421; (j) Lj. Manojlović-Muir, K.W. Muir, J. Organomet. Chem. 219 (1981) 129;

- (k) H.K. Yip, C.M. Che, S.M. Peng, *J. Chem. Soc., Dalton Trans.* (1993) 179.
- [25] (a) S.Z. Goldberg, R. Eisenberg, *Inorg. Chem.* 15 (1976) 535;
(b) N.M. Rutherford, M.M. Olmstead, A.L. Balch, *Inorg. Chem.* 23 (1984) 2833;
(c) T. Tanase, H. Ukaji, Y. Yamamoto, *J. Chem. Soc., Dalton Trans.* (1996) 3059;
(d) T. Tanase, K. Kawahara, H. Ukaji, K. Kobayashi, H. Yamazaki, Y. Yamamoto, *Inorg. Chem.* 32 (1993) 3682;
(e) W. Lin, S.R. Wilson, G.S. Girolami, *Inorg. Chem.* 33 (1994) 2265;
(f) Y. Yamamoto, H. Yamazaki, *Bull. Chem. Soc. Jpn.* 58 (1985) 1843;
(g) A. Modinos, P. Woodward, *J. Chem. Soc., Dalton Trans.* (1975) 1516.
- [26] T. Murahashi, T. Otani, E. Mochizuki, Y. Kai, H. Kurosawa, *J. Am. Chem. Soc.* 120 (1998) 4536.
- [27] K. Mashima, M. Tanaka, K. Tani, H. Nakano, A. Nakamura, *Inorg. Chem.* 35 (1996) 5244.